

Full length article

Strong electron-polarized atom chain in amorphous phase-change memory Ge–Sb–Te alloy

Nian-Ke Chen^a, Xian-Bin Li^{a, c, *}, Xue-Peng Wang^a, Wei Quan Tian^b, Shengbai Zhang^{a, c}, Hong-Bo Sun^a^a State Key Laboratory on Integrated Optoelectronics, College of Electronic Science and Engineering, Jilin University, Changchun, 130012, China^b College of Chemistry and Chemical Engineering, Huxi Campus, Chongqing University, Chongqing, 401331, China^c Department of Physics, Applied Physics, & Astronomy, Rensselaer Polytechnic Institute, Troy, NY, 12180, USA

ARTICLE INFO

Article history:

Received 17 June 2017

Received in revised form

2 October 2017

Accepted 5 October 2017

Available online 6 October 2017

Keywords:

Amorphous alloy

Structure-property relation

Phase-change memory

First-principles calculations

Atom chain

ABSTRACT

Phase-change memory (PCM) material is the promising material system for nonvolatile-memory technology. Performance optimization of PCM device urgently requires the deeper clarification of its material “Gene”. In this study, through first-principles calculations, *p*-orbital-aligned atom chains are identified to play important roles in governing optoelectronic reflectivity in amorphous Ge₂Sb₂Te₅. These atom chains make the electronic state of the amorphous Ge₂Sb₂Te₅ hold strong electron-polarized components, thereby governing the optical property. The present study offers a new understanding of “Gene” for PCM materials which benefit the material design and the performance improvement of PCM devices.

© 2017 Published by Elsevier Ltd on behalf of Acta Materialia Inc.

1. Introduction

Phase-change memory (PCM) is a state-of-the-art nonvolatile information storage technology which holds fast speed and high density [1–5]. It also shows potentials for flexible displays [6], thermal emitters [7], and brain inspired computing [8]. To functionalize its device, PCM material is reversibly switched between its crystalline and amorphous state accompanying with large optical/electrical contrast by laser or electrical pulse. To date, the ternary Ge–Sb–Te alloy has been one of the most popular PCM materials in applications [2,9]. It is critical to understand the “Gene” of the material to develop new systems with better performance.

As a prototypical composition, Ge₂Sb₂Te₅ (GST) has received extensive attentions. While the stable phase of the GST is hexagonal phase, the phase for storage is rock-salt phase that has 20% cation vacancies distributed randomly [10]. Recently, another crystalline phase with ordered vacancies has also been identified [11–15]. In general, the atoms in crystalline GST (c-GST) locate at octahedral

sites. A widely accepted bonding picture of c-GST is the resonant bonding model [16,17], which is induced by the aligned and half-filled *p* orbitals [18]. The delocalized electrons in resonant bonds lead to a large electronic polarizability and thus enhance the optical reflectivity in c-GST compared to the amorphous state. For amorphous GST (a-GST), its structure and bonding picture are complicated. Using X-ray absorption near-edge structure (XANES), Kolobov et al. demonstrated that Ge atoms located at tetrahedral sites with *sp*³ hybridization in amorphous phases [19]. By *ab initio* simulations, Caravati et al. revealed coexistence of the octahedral and tetrahedral sites of Ge atoms [20]. They further determined that in amorphous states two-thirds of Ge atoms preserve defective octahedral sites or pyramidal sites with bonding angles around 90° in addition to the rest (one third) with tetrahedral configurations. By Ge *K*-edge XANES analysis, Krbal et al. confirmed the coexistence of tetrahedral, pyramids, and distorted octahedral sites of Ge atoms in a-GST [21]. Using first-principles calculations, Akola et al. revealed the existence of ABAB rings and medium-sized cavities in a-GST [22]. Hegedus et al. demonstrated that the 4-fold rings and cubic motifs in amorphous state acted as nucleation seeds for fast crystallization based on *ab initio* molecular dynamics simulations [1]. The formation of large voids in amorphous GST was also discovered [23]. The “right angled” atomic motifs, such as the

* Corresponding author. State Key Laboratory on Integrated Optoelectronics, College of Electronic Science and Engineering, Jilin University, 2699 Qianjin Street, Changchun, 130012, China.

E-mail address: lixianbin@jlu.edu.cn (X.-B. Li).

pyramidal sites and the rings, was found to be originated from the dominant *p*-orbital bonding (dative bond) in amorphous states [24]. While the discussions above have shown different features for GST amorphous networks, the relation between its optoelectronic property and structure is still not clearly established, not mention to the “gene” of the material. To date, one of generally accepted knowledge is that electronic states in a-GST is much localized due to losing long-range order [16,18]. As such, its reflectance is significantly lower than that of crystalline phase, which defines a signal contrast for data storage.

In this article, through first-principles calculations and electronic structure analysis, the disordered network of a-GST is decomposed into specific motifs with different electronic properties. We find that a large amount of 3-atom chain motifs is identified to exist in a-GST. Unexpectedly, electrons in these chains can be strongly polarized even though in amorphous structure. As such the motifs can induce higher optical reflectivity. Our investigation provides a basic understanding of the relation between optoelectronic property and structure in amorphous PCM materials, which will help to design new candidates with desirable performance.

2. Simulation methods

All calculations are based on the density functional theory (DFT) with projected augmented plane waves (PAW) [25] pseudopotential and Perdew–Burke–Ernzerhof (PBE) exchange–correlation functional [26], as implemented in the VASP code [27,28]. A cubic rock-salt GST cell, which includes 43 Ge atoms, 43 Sb atoms, 108 Te atoms and 22 vacancies is used [10]. The calculated density for rock-salt GST is 6.0 g/cm³. The amorphous model is realized by the melt-quench technique. First, the crystalline model is diffused at 3000 K using NVT *ab initio* molecular dynamics (AIMD) for 6 ps to eliminate the initial setup. To obtain a reasonable liquid, an 18 ps NVT-AIMD simulation at 1100 K (close to the melting point) is run. Subsequently, the melt is quenched to 300 K with a rate of 13.3 K/ps. To calculate electronic properties, the final amorphous structure from AIMD is fully relaxed for better static balance position. The final density after relaxation is 5.6 g/cm³ which is about 6.4% smaller than the theoretically crystalline density of 6.0 g/cm³. The density contrast between crystalline and amorphous states is in consistent with the value of 6.8% in experiments [29]. The energy cutoff is 240 eV for static calculations and 180 eV for AIMD. The K-points for static self-consistent calculations and AIMD are $2 \times 2 \times 2$ and $1 \times 1 \times 1$ Monkhorst–Pack mesh, respectively. To analyze electronic polarization, an electron-density-distribution change (EDDC) is calculated according to a former study in thermoelectric materials [30]. The electron density distributions are respectively calculated without displacement and with a small displacement for a center atom. An EDDC is defined as the difference between the two densities. If the electrons are strongly polarized, the EDDC can have significant charge perturbations (by the displacement of the center atom) not only in the nearest neighbors, but also in the second or third neighbors along a chain. The displacement is ~2% of the length of two aligned bonds. Here, the atom chain is defined as an arrangement of atoms where their bond lengths are less than 3.3 Å and bond angles deviate less than 20° from a line (180°) in amorphous phase.

3. Results and discussion

Previous reports suggest the disorder GST contains particular local motifs [1,19–24]. The optoelectronic property of a-GST should be related to some local structures. To understand these local motifs, we should analyze their electronic properties. Here, we use a method called electron density distribution change (EDDC, the

electron density change, see the method section) which has been employed to qualitatively analyze electron-polarized bonds in thermoelectric materials, such as PbTe [30]. The EDDC in c-GST is first shown in Fig. 1(a)–(d). Similar to the phenomenon in crystalline PbTe [30], the EDDC in c-GST extends to not only the nearest neighbors but also the second (or even the third) neighbors along the linear chains from the central atom [displaced along the white arrow, see Fig. 1(b)]. In contrast, the EDDC in NaCl is just localized around the nearest neighbors (Fig. 2). Lee et al. [30] have demonstrated that the long-range EDDC can lead to long-range interactions between atoms in PbTe (i.e. strong electronic polarizability) which is absent in NaCl even with the same rock-salt structure. In other words, the long-range EDDC is not an artificial display. This long-range perturbation in c-GST indicates its significant electronic polarizability.

Fig. 1(c) further shows the EDDC from a central atom around intrinsic vacancies in crystalline GST. It is clear that the vacancy blocks the extension of the EDDC perturbation comparing to the case in Fig. 1(b). In other words, vacancies in c-GST can weaken electronic polarizability, which could be supported by the fact that the optical dielectric function in crystalline Ge–Sb–Te alloys decreases with increasing vacancy concentrations. For example, the imaginary part of dielectric function decreases significantly from Ge₂Sb₂Te₄ to Ge_{1.5}Sb₂Te₄ and further to Ge₁Sb₂Te₄ [31]. In Fig. 1(d), the center atom is displaced along diagonal direction, i.e. the [110] direction in (001) plane of the rock-salt structure. However, its EDDC perturbation still propagates along the *p*-orbital bonding direction [18]. This can be understood the [110] displacement can

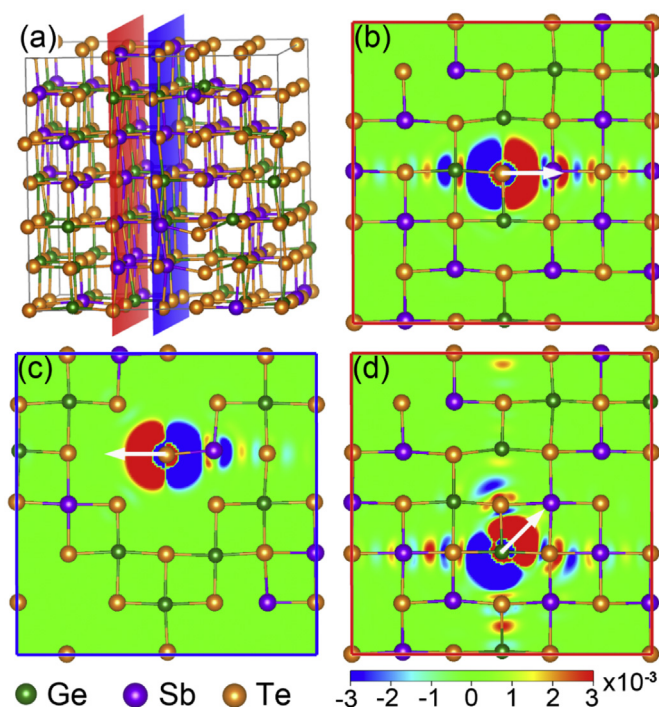


Fig. 1. The electron density distribution change (EDDC) induced by a displacement of central atom in c-GST. (a) 3D atomic structure of rock-salt c-GST. Two (001) planes are selected to analyze the EDDC. The red one corresponds to the EDDC in (b) and (d). The blue one corresponds to the EDDC in (c). (b)–(d) EDDC triggered by different displacements. The white arrows indicate the direction of displacement for a central atom. The starting points of the arrows mark the center atoms. The positive value of EDDC represents the increase of density while the negative value represents the decrease of density. The unit of charge density is $e/\text{Å}^3$. (For interpretation of the references to colour in this figure legend, the reader is referred to the web version of this article.)

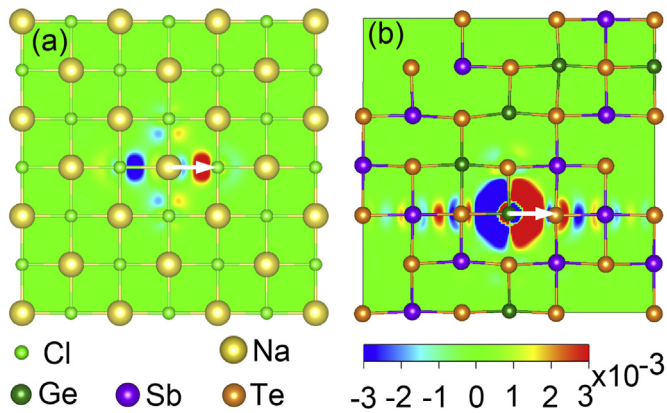


Fig. 2. Comparison of electron density difference change (EDDC) for (a) NaCl and (b) c-GST. The arrows indicate the direction of center-atom movements. The positive value of EDDC represents the increase of density, while the negative value represents the decrease of density. The unit of charge density is $e/\text{\AA}^3$.

be projected onto two vertical directions of [100] and [010] that trigger the EDDC perturbation along the two p -orbit directions, see Fig. 1(d).

According to previous reports [16,18], the strong electronic polarizability would be destroyed when long-range order is lost or structure localizations occurs. However, in this study even though the local vacancy can partly block the extension of the EDDC perturbation, there still remains an electronic-polarization characteristic to some degree (Fig. 1(c)). In other words, losing long-range order would not mean a complete destruction of large electronic polarizability for GST. To verify this hypothesis, an amorphous structure of GST is obtained by a melt-quenched molecular dynamics technique. Fig. 3(a) shows the amorphous structure. Here, a supercell with 194 atoms is adopted. The structural factor of the amorphous model is well consistent with those in experiment and previously reported AIMD simulations (Fig. 4) [20,22,32]. Indeed, we find that there are large amounts of atom chains remained in a-GST. These motifs are highlighted by thick sticks in Fig. 3(a). Besides a small amount (<10%) of the 4 or 5-atom chains,

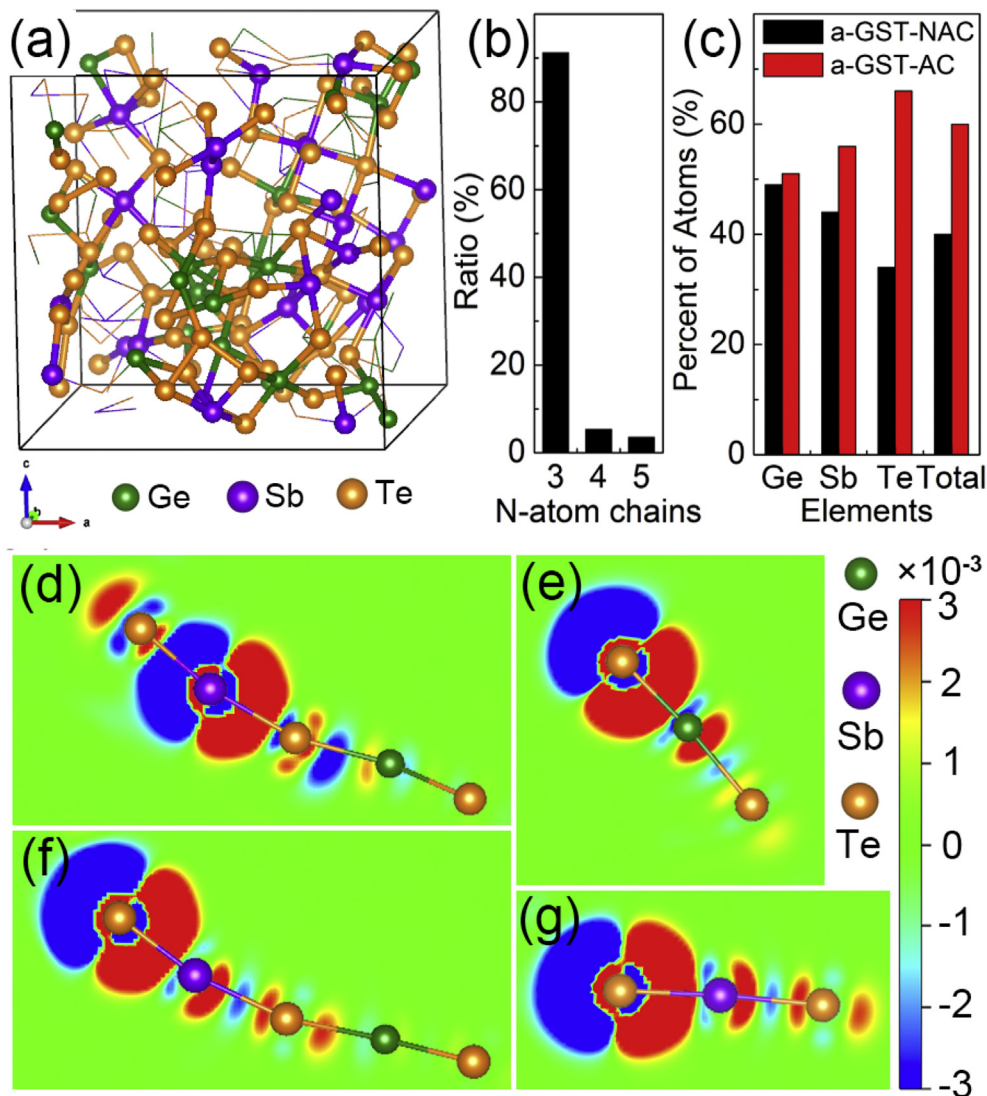


Fig. 3. The electronic polarizability of atom chains in amorphous GST. (a) The 3D atomic structure of a-GST. The amorphous network is displayed with thin lines. The atoms chains are highlighted by balls and thick lines. (b) The ratios of different kinds of atom chains. (c) The percent of atoms involved in atom chains. (d)–(g) EDDC of atom chains in a-GST. The positive value of EDDC represents the increase of density, while the negative value represents the decrease of density. The unit of charge density is $e/\text{\AA}^3$.

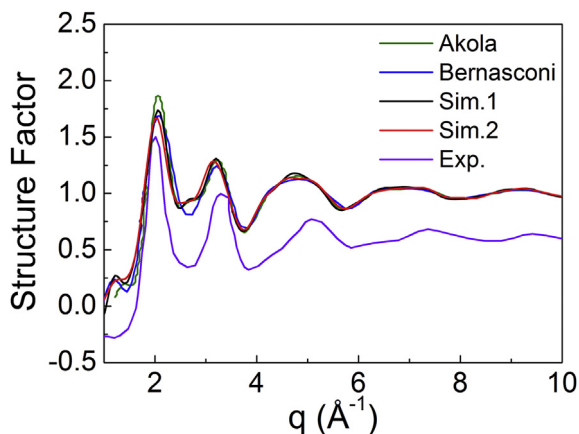


Fig. 4. The structure factors of four different amorphous GST models obtained with different quench rates: Akola model Ref. [22] 4.3 K/ps, Bernasconi model Ref. [20] 38.3 K/ps, our Sim.1 model 13.3 K/ps, and our Sim.2 model 30 K/ps. The experimental data is adopted from Ref. [32] and is shifted down by 0.4 for comparison. The calculated q-factors in our model are averaged by 1000 frames collected from a 300K-MD.

most of them are the 3-atom chains (Fig. 3(b)). In the amorphous model, 60% of all the atoms have involved in these atom chains (Fig. 3(c)) where Te atoms have the largest ratio and Ge atoms have the smallest ratio. However, more than half of the Ge atoms participate in forming atom chains. Therefore, the atom chain is an important feature in a-GST.

Fig. 3(d)–(g) further shows the electronic properties of these typical atom chains in a-GST. Similar to c-GST, a delocalized EDDC perturbation can be clearly observed, which implies an electronic-polarization characteristic also exists in amorphous state. Compared to previously reported motifs in a-GST (including tetrahedral Ge, the defective octahedral atom, or ABAB ring) [19–22], the motifs proposed here are more from the viewpoint of electronic characteristics but not only the structure. In fact, the 3-atom chain correlates with the medium-range order in amorphous GST, which can be reflected by its pair correlation function peaked at around 6 Å [1,22]. This peak is demonstrated here to indicate an effect of medium-range electronic correlation in the amorphous network. Before it is usually considered that just first-neighboring atoms have electronic correlation in a-GST.

To further demonstrate the relation between the optoelectronic signal (reflectance) and this atomic motif, the concentration of atom chains in amorphous phase is modified by a computational “experiment” where Ge atoms are replaced by other weak or non p -bonding elements. For example, Ge, Si, and C have a tendency to form the bonding from p type to sp^3 type in PCM materials. As such, two other new models can be created by replacing all the Ge atoms in a-GST by Si and C atoms, respectively. To see the change of local bonding and electronic behavior, the local balanced structures for the two models are obtained by geometry relaxations. Fig. 5(a) compares the bond-angle distributions for a-GST, amorphous Si–Sb–Te (a-SST) and amorphous C–Sb–Te (a-CST). Here, the peaks around 90° and 180° are the fingerprints of the p -orbit bonding and atom chains. It is clear that the peak of 90° (p bonding) changes to that of 109° (sp^3 bonding) and the peak of 180° gradually decreases from a-GST to a-SST and further to a-CST. Meanwhile, the numbers of atom chains in a-GST, a-SST and a-CST also decrease gradually (see Fig. 5(b)). The numbers of 3-atom chains in a-SST and a-CST are just 67% and 19% of that in GST, respectively. Correspondingly, the relative reflectance decreases significantly from a-GST to a-SST, and then to a-CST (Fig. 5(c)). To further confirm that the change of reflectance is due to the change of chains rather than only due to the change of chemical compositions, we compare the reflectance of the GST, SST, and CST models started from a rock-salt structure. Indeed, the reflectance of SST is close to that of GST because their number of chains are similar (see Fig. S1 and more details in the Supplemental Material).

In fact, a similar atomic motif named *3-center-bond* motif has been proposed [33,34]. This motif can be with $3c-2e$ bond (one short bond + one long bond) or $3c-4e$ bond (two short bonds). They have been pointed out to play an important role to form PCM crystal and makes the amorphization more energy efficient. Therefore, *3-atom chain* motif proposed here not only has the important impact on optoelectronic properties but also play a role on phase transition. In addition, the octahedral or pyramidal fragment [21] can be considered to be composed of several orthogonal atom chains. In other words, the existence of pyramidal fragment in amorphous GST also has a significant role to control optical properties of the amorphous GST.

To exam the reasonability of our present amorphous model and thus the results based on the model, we performed the second AIMD with a different quench rate of 30 K/ps. We also compare our models with other AIMD GST amorphous models from the literatures. In fact, the amorphous structures for our first simulation

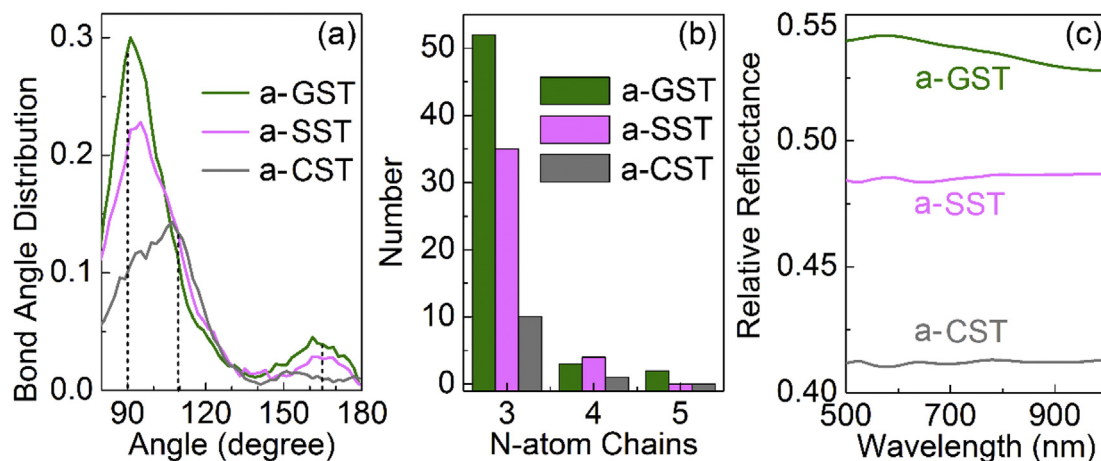


Fig. 5. (a) Bond angle distribution, (b) atom chains distribution and, and (c) relative reflectance of a-GST, a-SST and a-CST model.

model (sim.1) and the second one (sim.2) are almost the same: 60% total atoms and 54% total atoms participate to form atom chains for sim.1 and sim.2 models, respectively. Both their structure factors are also similar and in consistent with those from previous reports (see Fig. 4). Therefore, the amorphous model in this study is reasonable.

4. Conclusion

In this work, we identify that the 3-atom chain is an important structural motif in a-GST in term of electronic property. This motif has a strong electronic polarizability even in the disorder network. In contrast to the conventional purely electronic-localized covalent-bonding picture, the electronic-polarization characteristics (which is a fingerprint in crystalline state) is demonstrated to exist together with the localized bonding in amorphous PCM materials. A relation between the atom chains and optoelectronic reflectance is identified by a comparative analysis among a-GST, a-SST, and a-CST models. In this study, we stress that we do not deny the existence of covalent bonding in a-GST which should be the origin of reflectance contrast from its crystalline phase [35]. In fact, the advantages of PCM materials in memory are not just from their big difference between the two phases (to realize signal contrast) but also from their common points (to realize fast and reversible switch). The present research offers an updated understanding of the material gene in PCM materials which will benefit the new design of materials and the improvement of the performance in memory device.

Acknowledgements

Work at JLU, China was supported by the National Key Research and Development Program of China and National Natural Science Foundation of China (NSFC) under Grants #2017YFB1104300, #61590930, #2014CB921303, #11374119, #91423102 and #61775077. SBZ was supported by the Department of Energy under Grant No. DE-SC0002623. WQT thanks the support from the Open Project of Key Laboratory of Polyoxometalate Science of Ministry of Education (NENU) and State Key laboratory of Supramolecular Structure and Materials (JLU) (SKLSSM201723). The supercomputer time was provided by HPCC at JLU. This work is dedicated to 10-year establishment of *Lab of Computational Semiconductor Physics* in JLU (www.ioe-jlu.cn/csp).

Appendix A. Supplementary data

Supplementary data related to this article can be found at <https://doi.org/10.1016/j.actamat.2017.10.013>.

References

- [1] J. Hegedus, S.R. Elliott, Microscopic origin of the fast crystallization ability of Ge-Sb-Te phase-change memory materials, *Nat. Mater* 7 (2008) 399.
- [2] D. Lencer, M. Salinga, B. Grabowski, T. Hickel, J. Neugebauer, M. Wuttig, A map for phase-change materials, *Nat. Mater* 7 (2008) 972.
- [3] M. Wuttig, Phase-change materials: towards a universal memory? *Nat. Mater* 4 (2005) 265.
- [4] M. Wuttig, N. Yamada, Phase-change materials for rewriteable data storage, *Nat. Mater* 6 (2007) 824.
- [5] O.L. Muskens, L. Bergamini, Y. Wang, J.M. Gaskell, N. Zabala, C.H. de Groot, D.W. Sheel, J. Aizpurua, Antenna-assisted picosecond control of nanoscale phase transition in vanadium dioxide, *Light Sci. Appl.* 5 (2016), e16173.
- [6] P. Hosseini, C.D. Wright, H. Bhaskaran, An optoelectronic framework enabled by low-dimensional phase-change films, *Nature* 511 (2014) 206.

- [7] K.-K. Du, Q. Li, Y.-B. Lyu, J.-C. Ding, Y. Lu, Z.-Y. Cheng, M. Qiu, Control over emissivity of zero-static-power thermal emitters based on phase-changing material GST, *Light Sci. Appl.* 6 (2016), e16194.
- [8] T. Tuma, A. Pantazi, M. Le Gallo, A. Sebastian, E. Eleftheriou, Stochastic phase-change neurons, *Nat. Nanotechnol* 11 (2016) 693.
- [9] N. Yamada, E. Ohno, K. Nishiuchi, N. Akahira, M. Takao, Rapid-phase transitions of GeTe-Sb₂Te₃ pseudobinary amorphous thin films for an optical disk memory, *J. Appl. Phys.* 69 (1991) 2849.
- [10] T. Matsunaga, N. Yamada, Y. Kubota, Structures of stable and metastable Ge₂Sb₂Te₅, an intermetallic compound in GeTe-Sb₂Te₃ pseudo binary systems, *Acta Crystallogr. Sect. B* 60 (2004) 685.
- [11] V. Bragaglia, F. Arciprete, W. Zhang, A.M. Mio, E. Zallo, K. Perumal, A. Giussani, S. Cecchi, J.E. Boschker, H. Riechert, et al., Metal-insulator transition driven by vacancy ordering in phase change materials, *Sci. Rep.* 6 (2016) 23843.
- [12] I. Hilmi, A. Lotnyk, J.W. Gerlach, P. Schumacher, B. Rauschenbach, Epitaxial formation of cubic and trigonal Ge-Sb-Te thin films with heterogeneous vacancy structures, *Mater. Des.* 115 (2017) 138.
- [13] A. Lotnyk, S. Bernütz, X. Sun, U. Ross, M. Ehrhardt, B. Rauschenbach, Real-space imaging of atomic arrangement and vacancy layers ordering in laser crystallised Ge₂Sb₂Te₅ phase change thin films, *Acta Mater* 105 (2016) 1.
- [14] U. Ross, A. Lotnyk, E. Thelander, B. Rauschenbach, Direct imaging of crystal structure and defects in metastable Ge₂Sb₂Te₅ by quantitative aberration-corrected scanning transmission electron microscopy, *Appl. Phys. Lett.* 104 (2014) 121904.
- [15] B. Zhang, X.P. Wang, Z.J. Shen, X.B. Li, C.S. Wang, Y.J. Chen, J.X. Li, J.X. Zhang, Z. Zhang, S.B. Zhang, et al., Vacancy structures and melting behavior in rock-salt GeSbTe, *Sci. Rep.* 6 (2016) 25453.
- [16] K. Shportko, S. Kremers, M. Woda, D. Lencer, J. Robertson, M. Wuttig, Resonant bonding in crystalline phase-change materials, *Nat. Mater* 7 (2008) 653.
- [17] G. Lucovsky, R.M. White, Effects of resonance bonding on the properties of crystalline and amorphous semiconductors, *Phys. Rev. B* 8 (1973) 660.
- [18] B. Huang, J. Robertson, Bonding origin of optical contrast in phase-change memory materials, *Phys. Rev. B* 81 (2010) 081204R.
- [19] A.V. Kolobov, P. Fons, A.I. Frenkel, A.L. Ankudinov, J. Tominaga, T. Uruga, Understanding the phase-change mechanism of rewritable optical media, *Nat. Mater* 3 (2004) 703.
- [20] S. Caravati, M. Bernasconi, T.D. Kühne, M. Krack, M. Parrinello, Coexistence of tetrahedral- and octahedral-like sites in amorphous phase change materials, *Appl. Phys. Lett.* 91 (2007) 171906.
- [21] M. Krbal, A.V. Kolobov, P. Fons, J. Tominaga, S.R. Elliott, J. Hegedus, T. Uruga, Intrinsic complexity of the melt-quenched amorphous Ge₂Sb₂Te₅ memory alloy, *Phys. Rev. B* 83 (2011) 054203.
- [22] J. Akola, R.O. Jones, Structural phase transitions on the nanoscale: the crucial pattern in the phase-change materials Ge₂Sb₂Te₅ and GeTe, *Phys. Rev. B* 76 (2007) 235201.
- [23] Z. Sun, J. Zhou, A. Blomqvist, B. Johansson, R. Ahuja, Formation of large voids in the amorphous phase-change memory Ge₂Sb₂Te₅ alloy, *Phys. Rev. Lett.* 102 (2009) 075504.
- [24] M. Xu, Y.Q. Cheng, H.W. Sheng, E. Ma, Nature of atomic bonding and atomic structure in the phase-change Ge₂Sb₂Te₅ glass, *Phys. Rev. Lett.* 103 (2009) 195502.
- [25] G. Kresse, D. Joubert, From ultrasoft pseudopotentials to the projector augmented-wave method, *Phys. Rev. B* 59 (1999) 1758.
- [26] J.P. Perdew, K. Burke, M. Ernzerhof, Generalized gradient approximation made simple, *Phys. Rev. Lett.* 77 (1996) 3865.
- [27] G. Kresse, J. Furthmüller, Efficient iterative schemes for ab initio total-energy calculations using a plane-wave basis set, *Phys. Rev. B* 54 (1996) 11169.
- [28] G. Kresse, J. Furthmüller, Efficiency of ab-initio total energy calculations for metals and semiconductors using a plane-wave basis set, *J. Comput. Mater. Sci.* 6 (1996) 15.
- [29] W.K. Njoroge, H.-W. Wöltgens, M. Wuttig, Density changes upon crystallization of Ge₂Sb_{2.04}Te_{4.74} films, *J. Vac. Sci. Technol. A* 20 (2002) 230.
- [30] S. Lee, K. Esfarjani, T. Luo, J. Zhou, Z. Tian, G. Chen, Resonant bonding leads to low lattice thermal conductivity, *Nat. Commun.* 5 (2014) 3525.
- [31] M. Wuttig, D. Lusebrink, D. Wamwangi, W. Welnic, M. Gillessen, R. Dronskowski, The role of vacancies and local distortions in the design of new phase-change materials, *Nat. Mater* 6 (2007) 122.
- [32] S. Hosokawa, W.-C. Pilgrim, A. Höhle, D. Szubrin, N. Boudet, J.-F. Béjar, K. Maruyama, Key experimental information on intermediate-range atomic structures in amorphous Ge₂Sb₂Te₅ phase change material, *J. Appl. Phys.* 111 (2012) 083517.
- [33] A.V. Kolobov, P. Fons, J. Tominaga, Understanding phase-change memory alloys from a chemical perspective, *Sci. Rep.* 5 (2015) 13698.
- [34] A.V. Kolobov, P. Fons, J. Tominaga, S.R. Ovshinsky, Vacancy-mediated three-center four-electron bonds in GeTe-Sb₂Te₃ phase-change memory alloys, *Phys. Rev. B* 87 (2013) 165206.
- [35] C. Chen, P. Jost, H. Volker, M. Kaminski, M. Wirtsohn, U. Engelmann, K. Krüger, F. Schlich, C. Schlockermann, R.P.S.M. Lobo, et al., Dielectric properties of amorphous phase-change materials, *Phys. Rev. B* 95 (2017) 094111.